Design and Fabrication of Wireless Multilayer Tracking Marker for Intraoperative MRI-guided Interventions

Chim-Lee Cheung, Justin D.L. Ho, Varut Vardhanabhuti, Hing-Chiu Chang, Ka-Wai Kwok, *Senior Member, IEEE*

+

***Abstract*—This paper presents the design, fabrication, and evaluation of miniature magnetic resonance (MR)-compatible wireless markers, which can provide 3D positional tracking under magnetic resonance imaging (MRI). To achieve the small size of such markers, rectangular spiral planar coils were stacked in multiple layers, which can be fabricated on a flexible printed circuit board (FPC). Finite-element-based simulations and analytical modeling were applied to ensure proper adjustment of the MRI scanner resonant frequency, while maintaining a high circuit quality factor. A four-layer planar tracking coil was prototyped with a size of 6.7×1.5×0.3 mm^3, and a quality factor of 28.5. This design and fabrication approach are reportedly the first design to initiate wireless markers in such a small size, enabling straightforward integration with interventional tools. When validated under MRI, the tracking marker appeared as a very high contrast spot on the MR images. For a 48 mm distance from the isocenter, the estimated maximum errors in 3D position was 0.48 mm. And the inherent standard deviation of marker localization was 0.12 mm. With the high MR contrast signal generated, the presented markers enable automatic and real-time tracking in 3D, but without MR image construction. In combination with the small form-factor, this marker would facilitate MRI-guided navigation of interventional tools, in particular for those assisted by tele-operated robots.**

***Index Terms*—Magnetic resonance imaging (MRI), position measurement, medical robotics, robot sensing system, coils.**

I. Introduction

MAGNETIC resonance imaging (MRI) guided navigation plays an increasingly important role in reshaping current interventional practices that employ computed tomography (CT) or X-ray fluoroscopy. This is attributed to the unique advantages of MRI, such as zero ionizing radiation and high-contrast visualization of soft tissues and their physiological details [1]. Despite many benefits of MRI-guided interventional approaches, there are several difficulties that inhibit its widespread use in clinical practice. The primary difficulty lies in the device localization of surgical instruments in the MRI system, for which the extremely strong static magnetic field inside the MRI bore limits the choice of approach. This makes the design and fabrication of MR (magnetic resonance) conditional devices very complicated. Any improper electromagnetic (EM) signal generated during the MRI causes significant artifacts, which can distort and deteriorate overall image quality.

Furthermore, It is technically challenging to employ tracking systems outside the MRI bore, such as optical camera tracking [2] as used in conventional image-guided intervention. These optical systems have to be placed further from the scanner, while also maintaining line-of-sight with the reflective optical markers linked with instruments inside the MRI bore. Recently, advances of optical fiber Bragg grating (FBG) sensors [3] allow it to be mounted onto an instrument/catheter spline to frequently measure its shape along its length. However, this FBG-tracked shape is not necessarily well-aligned/registered with the MR images. Rigid registration of FBG-based tracking with MRI would be found difficult because of the MR image distortion inevitably induced by the inhomogeneity of background field and nonlinearly varying gradient field, that can be somehow up to 24 mm over a 24 cm field of view for 1.5T magnet [4] . Therefore, much research attention has been shifted to positional tracking carried out by the MRI system itself.

To localize surgical instruments in the MR image domain, conventional passive tracking markers can be employed, which capsulize either negative [5, 6] or positive [7, 8] contrast materials. These markers provide remarkable intensity changes in MR images, however, their use may involve complicated MR sequences [9] to contrast the signal from the foreground images. It would also take significant computation time to process or recognize susceptibility artifacts in high-resolution images, which is impractical for the aim of automatic, real-time marker tracking. This passive approach may also encounter difficulties when multiple markers are close to each other, or even if they are out of the imaging site/slice.

Real-time, active tracking, achieved by MR-based radiofrequency (RF) coil markers [10], becomes the pre-requisite for providing fast, robust positional feedback in situ in MR image coordinates [11]. It is particularly useful for robot-assisted approaches by closing the feedback control loop of any robotic system [12]. It would add confidence to the operator (in the control room) who tele-manipulates instruments (e.g. needle, catheter [13, 14] and stylet), and drives them towards target lesions. The instrument configuration and the desired targeting path can also be

This work is supported in parts by Signate Life Sciences Limited, the Croucher Foundation and the Research Grants Council (RGC) of Hong Kong (Ref. No. 27209515, No. 17227616, and No. 17202317).

C.L. Cheung, J.D.L. Ho, and K.W. Kwok are with Department of Mechanical Engineering, The University of Hong Kong, Hong Kong (corresponding author to provide phone: +852-3917-2636; e-mail: kwokkw@hku.hk).

V. Vardhanabhuti, H.C. Chang are with Department of Diagnostic Radiology, The University of Hong Kong, Hong Kong,

This article has been accepted for publication in a future issue of this journal, but has not been fully edited. Content may change prior to final publication. Citation information: DOI 10.1109/TMECH.2020.2970990, IEEE/ASME Transactions on Mechatronics

TABLE I
MINIATURIZED COILS FOR MAGNETIC RESONANCE IMAGING TRACKING

SOURCES [REF]	DESIGN	FABRICATION TECHNIQUE	WORKING FREQUENCY (MHZ)	SIZE IN MM (LENGTH*WIDTH*HEIGHT) (DIAMETER*LENGTH)	COMMENTS
[25]	Solenoid coil	Wire wound	63.87	3 × 3 × 5	Internal signal source is needed. Complicated wire winding process.
[28]	Planar rectangular spiral coil	Wire wound	63.87	15 × 2.6 × 0.2	Complicated wire winding process.
[29]	Solenoid coil	Wire wound	127.7	4 × 3	Internal signal source is needed. Complicated wire winding process.
[23]	Single loop coil	Hot embossing	127.7	13 × 1.57 × 0.2	Difficult to achieve compact size.
[24]	Planar square spiral coil	Lithography	63.87	17 × 2 × 0.055	High reproducibility with precise fabrication procedure.
[34]	Split-ring resonators	Microfabrication	123	8 × 8 × 0.115	High flip angle (i.e. 6-18°) is needed.

precisely overlaid on the intra-operative (intra-op) MR images to enhance visual feedback. Such tracking mostly utilizes a limited number of coil units wired/connected to a receiver electronic system through coaxial cables. The coil units can actively "pick up" the MR gradient field [15] along the three principal directions. Their individual 3D coordinates can be calculated/localized from tracking pulse sequences using 1D projection readouts. This 3D localization can be completed within a few milliseconds, thus enabling a high tracking rate. The optimal tracking performance can be attained at a high resolution of 0.6×0.6×0.6 mm^3, and at a high sampling rate at 40 Hz [16]. Although active methods can provide robust tracking of coils, their conductive wires/cables would act as a radio-frequency (RF) antennae, generating heat that can damage the surgical instrument or harm the patient [17, 18]. This heating problem may be resolved by quarter-wavelength coaxial chokes [19], or transformers added to the transmission line [20], but this would further complicate the integration of the tracking system.

Another proposed tracking method is semi-active tracking. Optical fiber, unlike conductive wires/cables, is employed to connect with the coil tracking unit. The fiber can deliver variable light that alters the resonant frequency of the coil unit [21, 22] by including a photodiode in the coil circuit. The resonance effect with the MRI system can then be switched ON/OFF. However, extra components, such as the photodiode and optical fiber lens, inevitably increase the overall size of the tracking units, which may make its integration difficult.

To this end, wireless tracking markers have been proposed and applied very recently [23-30], which are circuits specialized for amplifying MR signal with low-flip angle pulse sequence. It does not require additional hardware or electric wire connection with the MRI system, but instead inductively couples to the scanner's RF coils. Due to the absence of long co-axial wires, the risk of RF-induced heating [31-33] can be minimized. Real time tracking can be attained at 30 Hz [28, 29], and the high signal-to-background ratio allows rapid localization by using 1D-projection technique. However, a major hurdle is the integration of wireless markers with surgical instruments, which requires small size but still sufficient quality factor. As such, the miniaturized design and fabrication method of such markers has become a timely research issue.

In this paper, we propose a new design and fabrication approach of a tiny and thin wireless MR-tracker marker (6.7 mm × 1.5 mm × 0.3 mm), much smaller than those seen in prior art (as in **TABLE I**), but with a quality factor (Q factor) still comparable to them. Our work contributions can be well-differentiated below:

i) It is an original and innovative design that utilizes a multilayer inductor structure for miniaturization. This approach significantly improves the inductance-to-resistance ratio, thus the quality factor, for a given outer dimension. It presents a new direction for future miniaturized wireless marker design.
ii) Detailed analytical modeling and finite element analysis (FEA) is performed to characterize the multilayer wireless marker's performance. Accurate and repeatable fabrication is realized by a flexible printed circuit (FPC) design.
iii) Experimental evaluation of the MR-tracking performance using pulse sequences was conducted under a closed-bore 1.5-T scanner. RF-induced heat was also verified to ensure MR safety according to ASTM protocol [35].

II. METHODS AND MATERIALS

A. Miniaturization and Quality factor

The wireless marker must resonate at the MRI Larmor frequency f_L to amplify the B_1 field. Referring to [36], the resonant frequency of the marker with inductance L, capacitance C can be written as

$$f_m = \frac{1}{2\pi\sqrt{LC}} \tag{1}$$

It can be seen a lower resonant frequency requires larger inductance and capacitance values, which essentially leads to larger circuit size. On the other hand, the MR signal amplification depends on the circuit's quality factor

$$Q_m = \frac{1}{R}\sqrt{\frac{L}{C}} = \frac{2\pi f_L L}{R} \tag{2}$$

Note that the quality factor depends linearly on the ratio L/R of the marker. Therefore, typical miniaturization approaches like decreasing number of inductor turns, inductor outer dimensions, or even diameter of conductor [28] inevitably leads to a lower L/R ratio, hence the marker's amplification performance. Therefore, a new marker design approach is necessary for miniaturizing the marker with no degradation of the quality factor.

This article has been accepted for publication in a future issue of this journal, but has not been fully edited. Content may change prior to final publication. Citation information: DOI 10.1109/TMECH.2020.2970990, IEEE/ASME Transactions on Mechatronics

The prototype and schematic diagram of the proposed MR tracking marker is shown in **FIG. 1**. The marker comprises of four conductive copper layers that are stacked vertically to form a 3D multilayer configuration. It can be divided into two main parts: **I)** multiple layers of planar rectangular spiral inductors on FPC boards electrically connected by multiple through-hole vias, and **II)** Two rectangular conductive pads that are arranged for soldering a non-magnetic surface-mounted capacitor (0.6 mm × 0.3 mm × 0.3 mm, KEMET, US). To achieve miniaturization while maximizing the sensitive area over the area surface, a rectangular planar design has been adopted.

The principle and configuration of the developed tracking marker take advantage of the additional inductance introduced and even the mutual coupling effect between the multiple layers, as shown in **FIG. 1(c).**

$$L_{total} = L_1 + L_2 + L_3 + L_4 + M_{1,2} + M_{1,3} + M_{1,4} + M_{2,3} + M_{2,4} + M_{3,4} \quad (3)$$

where L_i is the self-inductance of each layer, and $M_{i,j}$ is the mutual inductance induced between two layers i and j. The accumulated self-inductance from each layer is further amplified because their generated magnetic flux passes through other stacked layers, thus significantly magnifying the total inductance within the same footprint. The marker resistance can be approximated as

$$R_m = \frac{\rho_c \cdot l_c}{w \cdot b_c} \quad (4)$$

where l_c is the total trace length, ρ_c is the trace material resistivity, b_c is the trace thickness, and w is the trace width. Note that the additional resistance contributed from extra conductive traces grows linearly with l_c. As a result, the L/R ratio can be significantly increased by multiple layers stacking. Since the conductors were only stacked vertically, the total area of the coil remains unchanged. The planar form of marker is kept since the length of the tracking marker (6.7 mm) is still much larger than the overall thickness (0.3 mm). Although in theory more stacked layers can improve the quality factor, we limit the maximum layer to 4 for a proof-of-concept study.

The presented marker will become an integral part of an interventional instrument, e.g. catheter, stylet, or needle (OD < 3 mm). This constrains the overall size of the marker, with the maximum width limited by the cylinder diameter. In this work we define 1.5 mm as the marker width for a 3 mm diameter stylet [16] to construct the inductor.

Compared to existing MR fiducial markers, the presented design has several advantages. Firstly, it significantly enhances the marker's total inductance and quality factor within the same footprint, enabling a smaller marker surface while ensuring sensitive MR signal detection for automatic tracking. Secondly, the tedious tune-and-match process [25, 28, 29] can be avoided, which was to compensate for fabrication errors particularly for manually wound coils. The configuration of markers can also be precisely adjusted to integrate with various interventional tools. Finally, comparing to previous markers that were wound around a capsule filled with internal signal source, the marker can amplify the MR signal through surrounding in-vivo tissue, or even in combination with a signal source for ex-vivo operation.

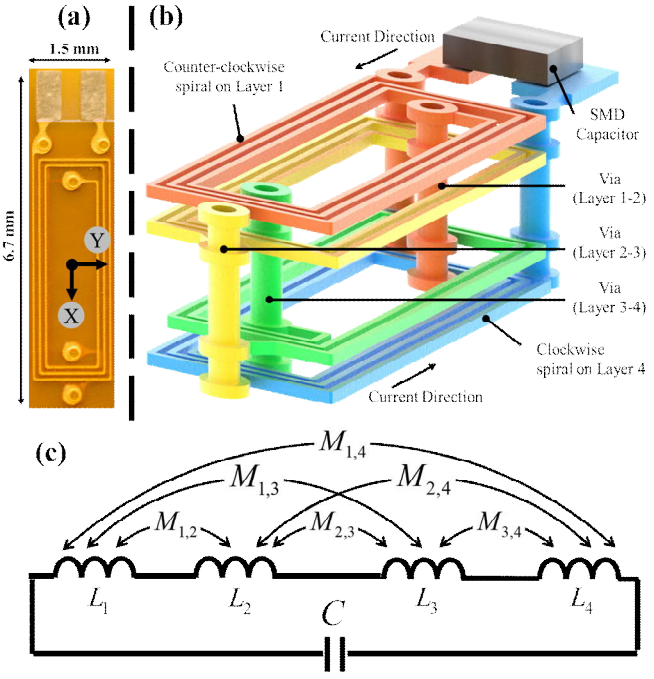

Fig. 1 Multilayer design of the MR tracking marker. **(a)** Real prototype stacked with four layers of coils. Each comprises of three turns of coils with outer dimensions 6.7 mm × 1.5 mm. **(b)** 3D schematic of marker: rectangular traces (in orange, yellow, green, blue) denote the copper conductor, and the hollow circles are plated-through-hole to provide conductive connections between layers. **(c)** Multiple stacked layers utilize the mutual coupling effect to introduce additional inductance within same 2D footprint.

B. *Fabrication and Characterization*

In prior art of MR fiducial marker designs, the use of solenoid inductors is predominant. They were typically wrapped on the cylindrical surface of catheters [37] or around a dedicated signal source [25]. It is advantageous that the fabrication of solenoid coils does not require high-end machinery, however its handling could be tedious and labor intensive, particularly when the coil has an embedded internal signal source. In most cases, a manual tuning-and-matching procedure is required, which adversely affects its reproducibility. Fabrication with FPC was adopted which is already the standard ready for mass production. Copper and polyimide were chosen as they are MRI-conditional and -safe materials. The fabrication was divided into two main steps. First, two double-layer FPC boards were made separately. For each board, copper traces were printed on the opposite side of a polyimide substrate, and the two sides were electrically connected in series by a plated-through-hole. On top of the copper traces, a thin coverlay layer was then overlaid to ensure good insulation and protection for the copper traces. Secondly, the two boards were bonded together with a thin layer of epoxy, thus forming an integrated multilayer coil. Key design parameters of the tracking markers are tabulated in **TABLE II.**

After the fabrication of the multilayer inductor, S11 reflection coefficients of the multilayer inductor were measured by using a Vector Network Analyzer (E5071A, Keysight Technologies, US) to electrically characterize the inductor alone. Afterwards, a non-magnetic surface-mounted capacitor was selected to tune the whole circuit to 63.87 MHz (1) at no-load condition and was soldered to the rectangular conductive pads.

This article has been accepted for publication in a future issue of this journal, but has not been fully edited. Content may change prior to final publication. Citation information: DOI 10.1109/TMECH.2020.2970990, IEEE/ASME Transactions on Mechatronics

TABLE II
DESIGN SPECIFICATIONS OF THE MULTILAYER INDUCTOR

PARAMETERS	SYMBOL	VALUES
Maximum coil outer diameter	d_{out}	5 mm
Minimum coil inner diameter	d_{in}	0.53 mm
Minimum conductor width	w	0.06096 mm
Minimum conductor spacing	s	0.06096 mm
Conductor thickness	b_c	12 um
Conductor material properties (resistivity, permeability)	ρ_c, μ	~ 17 nΩm, 1
Adhesive thickness	b_{ad}	25 um
Adhesive dielectric constant	ε_{ad}	3.5 (epoxy)
Coverlay thickness	b_{cov}	27.5 um
Substrate thickness	b_s	25 um
Substrate dielectric constant	ε_s	3.5 (polyimide)

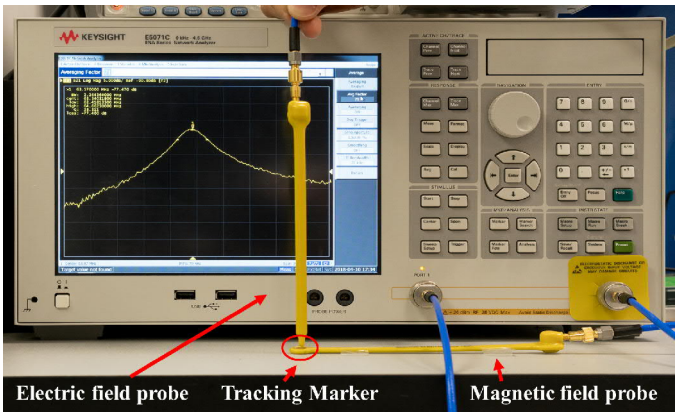

FIG. 2. Non-contact probing using an RF measuring tool, vector network analyzer (VNA). RF resonant performance was measured. The proposed wireless tracking marker was placed between the magnetic field probe and the electric field probe.

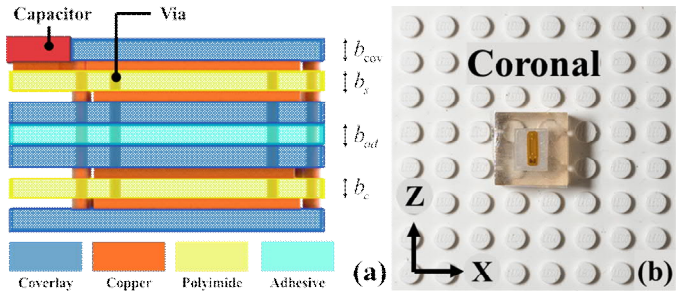

FIG. 3. **(a)** Schematic diagram showing the electrical connection and the architecture of a marker with 4 layers. The design parameters are defined referring to **TABLE II**. **(b)** Wireless tracking marker mounted on a 3D-printed block filled with agar gel placed on coronal plane.

In this study, the marker was sealed with medical grade adhesive (209-CTH, Dymax, United States) to provide electrical insulation. With the tracking marker assembled and sealed, it is difficult to simply connect it to the VNA through a coaxial cable. We measure the scattering parameter of the assembled marker by non-contact probing as shown in **FIG. 2**, and there is no direct electrical connection between the assembled marker and the probes. The non-contact probing setup mainly consists of a magnetic field probe (100A, Beehive Electronics, US), and an electric field probe (100D, Beehive Electronics, US).

C. MR Tracking and Orientation Dependency tests

The 3D tracking performance of the wireless tracking marker were evaluated inside a clinical 1.5T MRI scanner (Signa HDx, Software Release 16.0_V02, GE Healthcare, Waukesha, WI, USA) with a standard 8-receiver imaging head coil. As can be seen in **FIG. 3b**, the setup included a single marker put on a phantom filled with agar gel. The marker was mounted on a standard 16×16 Lego plate with 8-mm step size. The setup was fixed stationary on the scanner bed with adhesive tape and aligned with the scanner coordinate system by using the positioning laser.

The accuracy and precision of the marker was accessed from the MRI images with the sub-pixel localization method [38], in which intensity linear interpolation (ILI) method was employed to calculate the marker position. The method initially finds two coordinates with half-maximum intensity value along an axis, with the mean of the coordinates representing the marker center in that dimension. The MRI images (**FIG. 9**) were acquired with a gradient echo (GRE) sequence, of which the settings are TE = 4.472 ms, TR = 10.15 ms, slice thickness = 0.6 mm, matrix = 224 × 224, flip angle = 1°, FOV = 135 mm × 135 mm, pixel spacing = 0.527 mm. Gradient warp correction was also applied to compensate the image distortions caused by gradient nonlinearities. The scanned MR images were exported in DICOM format and processed in MATLAB (MathWorks, Natick, MA, USA).

Thirty images were taken on the same plane as the isocenter and averaged as the baseline image for later comparison. Six images at a step size of 16 mm were taken along the *x*- and *z*- direction of the Lego plate (**FIG. 3b**), individually, for post-processing in MATLAB. As the RF and gradient coils have principle symmetry with respect to *x* and *y* axes, we assume the *x* and *y* coordinates have the same positional errors; therefore, we did not measure the *y* coordinate separately. Note that a shorter update time of tracking, 35 ms [29], is achievable by utilizing short 1D projection along the three-principle axis with comparable accuracy and precision [29].

The wireless marker has the maximum signal coupling with MRI scanner when its normal axis is perpendicular to the main magnetic field B_0, and no coupling when its normal axis is parallel to B_0. The orientation dependency was tested by placing the marker horizontally on a custom-made MRI compatible rotary mount. The marker's normal Z-axis (**FIG. 1a**) was initially perpendicular to B_0 field at 0°. A protractor was used to adjust the marker's normal axis against the B_0 field on the sagittal plane from 0° to 90° in steps of 15°.

D. Radiofrequency Safety Test

The multilayer marker is not disabled and can resonate during RF excitation, so it may induce RF heating that pose hazard to human. RF-induced heating of the tracking marker was evaluated according to the ASTM protocol (ASTM F2182-09) [35]. The heat was measured with two factory calibrated fiber-optic fluorescent temperature sensors with 0.01 °C resolution connected to a measurement logging unit (PRB-MR1-10M-STM-MRI, OSENSA, Canada). The fibers were channeled through a waveguide between the MRI room

This article has been accepted for publication in a future issue of this journal, but has not been fully edited. Content may change prior to final publication. Citation information: DOI 10.1109/TMECH.2020.2970990, IEEE/ASME Transactions on Mechatronics

and control room. The temperature measurements were sampled at a rate of 33 Hz. One sensor was set on top of the marker to collect temperature directly, and one sensor was set on the patient table as reference [16, 28, 29, 34, 39]. A fast-spin echo imaging sequence was repeated for approximately 15 minutes on the aforesaid 1.5T MRI scanner with TE = 8.38 ms, TR = 600 ms, ETL = 40, slice thickness = 20 mm, Matrix = 256×256, FOV = 410 mm×410 mm, and flip angle = 90°. The sequence was set with high flip angle at 90° to provide large thermal effect and induced a whole-body average specific absorption rate (SAR) of 2 W/kg.

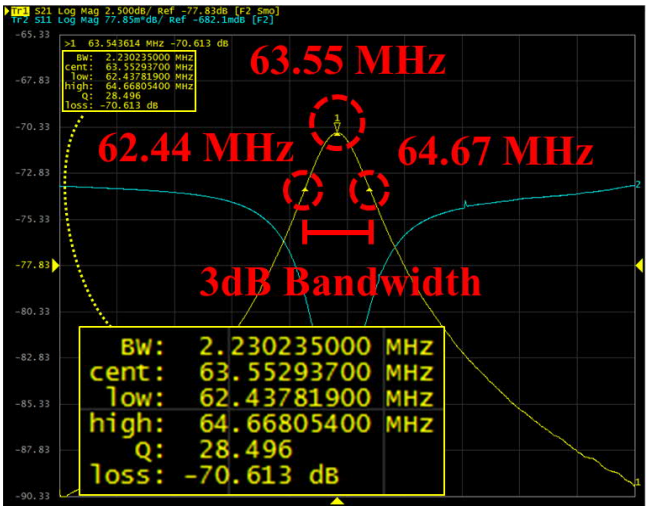

FIG. 4. Scattering measurement of the assembled wireless tracking marker. Both S11 reflection coefficient (indicated by the blue line) and S12 transmission coefficient (yellow line) are measured. Quality factor is calculated by measuring the 3dB bandwidth ratio of the S12 magnitude (indicated by the two red circles).

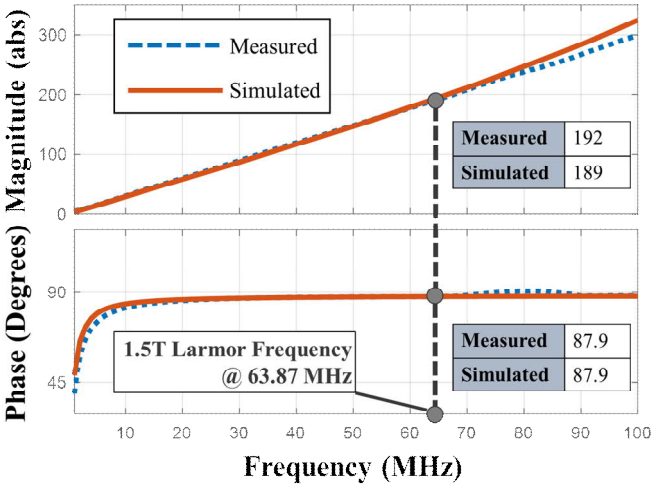

FIG. 5. Measured and FEM simulated impedance of the multilayer planar spiral inductor. The results are in good correspondence from 1 to 100 MHz. The vertical gray line indicates the 1.5T Larmor Frequency.

III. Result and Discussion

A. Characterization and Finite Element Analysis (FEA)

The scattering parameters measured in both S11 mode and S12 mode using wireless measuring probes is depicted in **FIG. 4.** A peak can be found at 63.55 MHz of the transmission coefficient, with a corresponding quality factor of 28.5. The quality factor was computed by dividing the resonant frequency by the 3dB bandwidth. The resultant resonant frequency had 0.5 % error from the desired value, which could

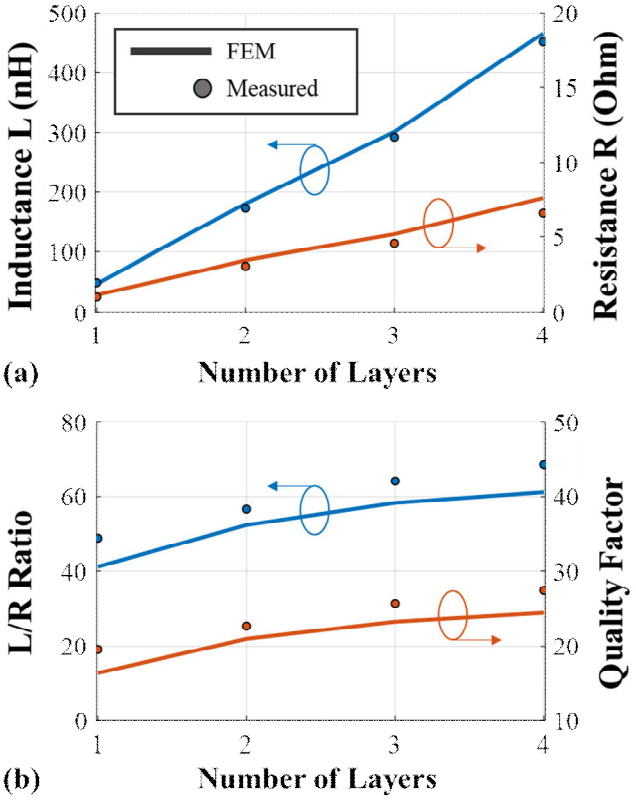

FIG. 6. (a) Measured inductance and resistance of the proposed multilayer planar inductor. **(b)** Calculated Inductance-to-Resistance ratio and the resultant quality factor.

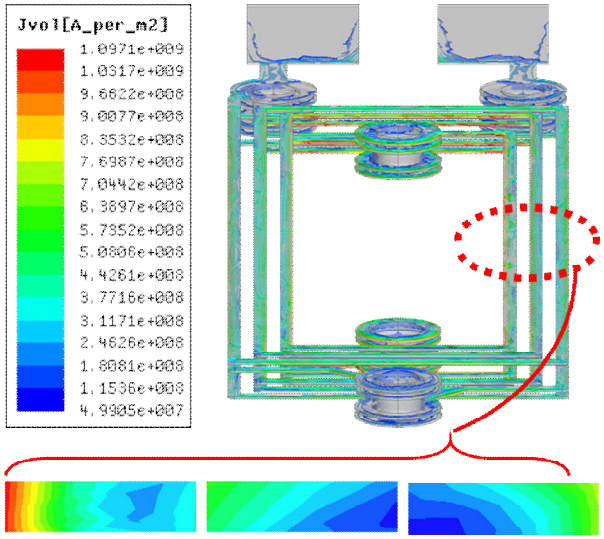

FIG. 7. Electric current density in the cross-section of multilayer planar inductor, with an input current of 1 A at 63.87 MHz.

be attributed to the manufacturing tolerance of the capacitor, and additional parasitic elements from the soldering joints.

Although several closed-form equations [40-46] have been proposed in literature, which were applied to approximate the inductance of planar spiral coil, currently, there is no readily available expression for multilayer planar coils with rectangular spiral geometry. The combination of multiple flexible winding structures makes the electrical characteristics of the multilayer inductor difficult to be analytically approximated. Precise estimation of the planar coil was carried out with an electromagnetic field simulation (HFSS, Ansoft Corp., Pittsburgh, USA). The HFSS software is based

This article has been accepted for publication in a future issue of this journal, but has not been fully edited. Content may change prior to final publication. Citation information: DOI 10.1109/TMECH.2020.2970990, IEEE/ASME Transactions on Mechatronics

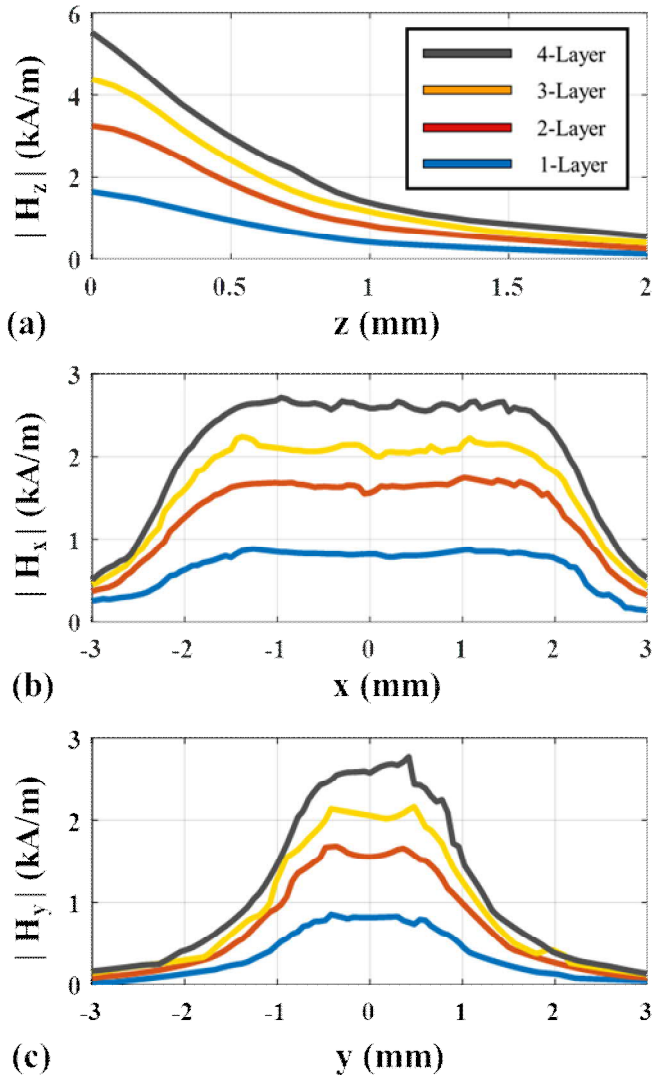

FIG. 8. Sensitivity profiles for inductors with different number of layers along the **(a)** *z*-axis, **(b)** *x*-axis at z = 0.6 mm, and **(c)** *y*-axis at z = 0.6 mm.

on finite element methods to predict the full-wave performance of a defined structure under electromagnetic circumstance. Taking advantage of the FEA, we quantitatively estimate the inductance and AC impedance of the multilayer inductor.

The simulation setup contained a MR tracking marker placed inside an air phantom (20 mm × 20 mm × 20 mm). An excitation of 1-V continuous wave signal at 63.87 MHz (1.5T Larmor frequency) was applied at the terminal of the multilayer inductor. To verify the simulation, inductors with different number of layers were fabricated and then characterized by the VNA to determine the electrical parameters. **FIG. 5** shows an example of the simulations in which the simulated and measured impedance of a 4-layer planar spiral inductor were plotted from 1 MHz to 100 MHz.

To show the merit of the novel multilayer design, **FIG. 6 (a)** shows the VNA measured and FEA simulated inductance and winding resistance of the proposed multilayer planar inductor. It can be observed that as the number of layers increased from one to four, the total inductance increased by approximately 9.1 times. On the other hand, the total resistance increased by 6.5 times, which is more than 4 times as expected in (4). This can be explained by the skin effect that leads to a non-uniform

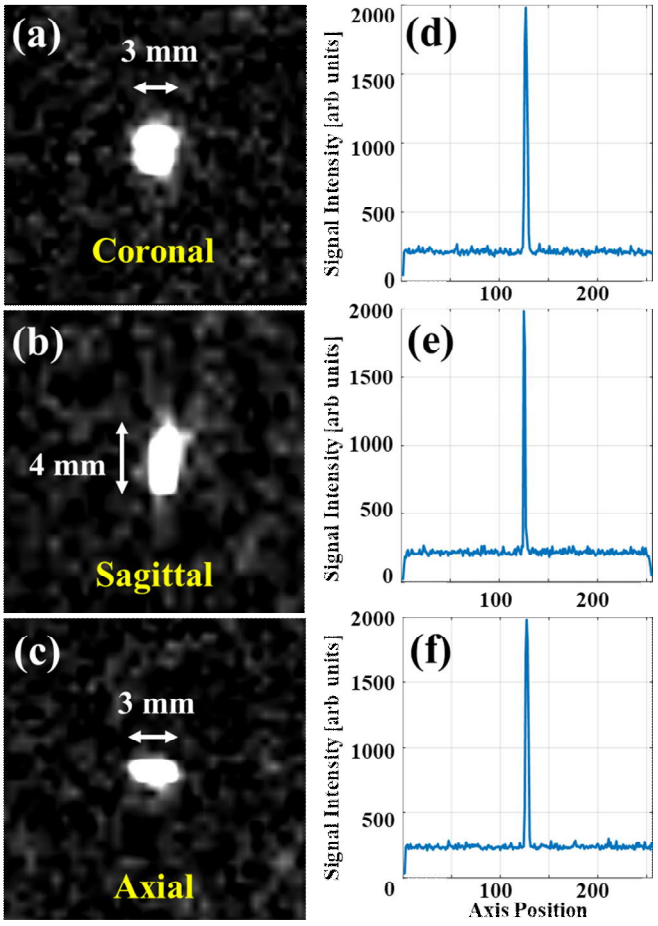

Fig. 9. (a) Coronal, **(b)** Sagittal, and **(c)** Axial low flip angle (1°) GRE images of the wireless marker. The marker amplifies the MR signal in its vicinity, resulting in high marker-to-background signal contrast. **(d-f)** Maximum signal intensity plot in the corresponding planes.

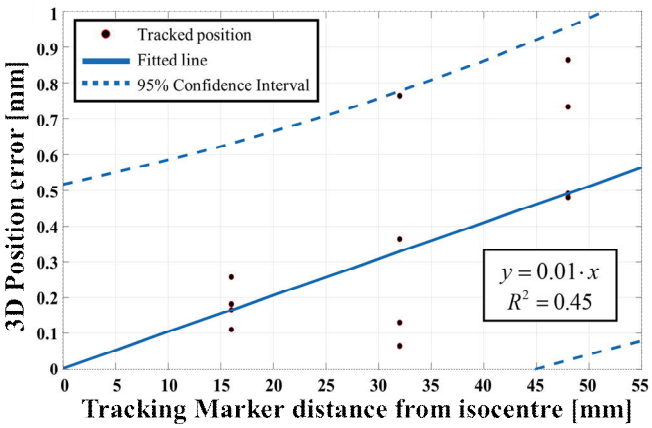

FIG. 10. Calculated 3D position error of the tracking marker against its distance from the isocenter. The data points were fitted with a solid line that intercepts at the zero point. The short-dashed lines indicate the 95% confidence interval.

current distribution inside the copper conductor [47]. The proximity effect is also present between the conductors, in which the current is concentrated in the remote half portion of the copper. As a result, the current tends to flow near the surface of the conductor as shown in **FIG. 7**, therefore the effective cross section $w \cdot b_c$ is reduced. However, as the percentage increase of inductance is larger than that of the resistance, the overall quality factor increased with additional layers as shown in **FIG. 6(b)**.

This article has been accepted for publication in a future issue of this journal, but has not been fully edited. Content may change prior to final publication. Citation information: DOI 10.1109/TMECH.2020.2970990, IEEE/ASME Transactions on Mechatronics

To understand the RF field pattern differences created from a multilayer configuration, inductors with a different number of layers but with the same planar dimensions (4.5 mm × 1.5 mm) were modelled and simulated. H-field sensitivity profiles according to the coordinate system in **FIG. 1a** were calculated at the center of coils, with an excitation current of 1 A as shown in **FIG. 8.** It can be observed that increasing the number of layers can provide a stronger H-field near the coil. On the z-axis, at z = 0.6 mm, the values of H-field of all designs drops to about 50% of the highest value at z = 0 mm. **FIG. 8b-c** shows the H-field along the *x*- and *y*-axis respectively at z = 0.6 mm. The results show that increasing the number of layers can also introduce a larger sensitive range, which implies a larger volume near the marker with amplified flip angle.

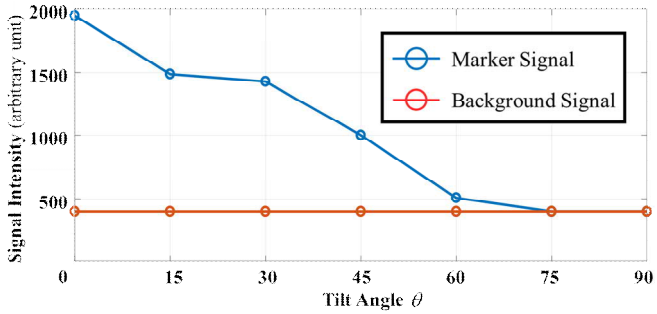

Fig. 11. Marker's signal intensity dependence on tilt angle θ. With GRE pulse sequence, the marker can be differentiated from background for a tilt angle up to 60°.

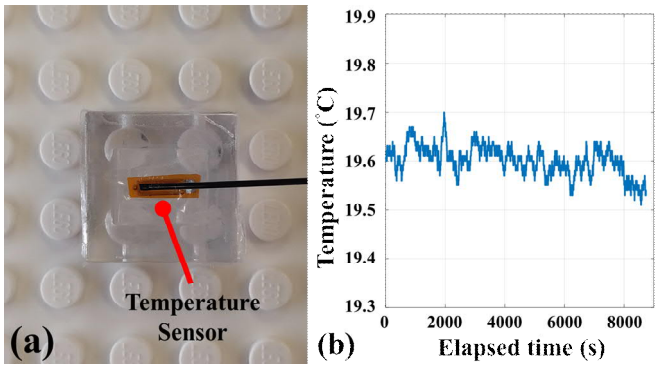

FIG. 12. Temperature measured on the MR tracking marker over a 15 min FSE: **(a)** an optical thermometer probe was directly attached to the marker's surface. A second sensor was set on the patient table as reference. **(b)** Calibrated temperature change of the marker. The maximum change in temperature was < 0.1 °C.

B. MR Tracking and Orientation Dependency

Fig. 9 demonstrates the marker's local signal enhancement effect at low flip angle pulse sequence, resulting in a sharp contrast between the marker's vicinity and the background. Images with the highest peak-to-noise ratio were selected from the receiver channel for the marker's tracking performance analysis. To indicate the inherent precision of the tracking procedure, the ILI algorithm was applied to the baseline image, obtaining a standard deviation of 0.12 mm (0.26 pixel). Results of the accuracy measurement are plotted in **FIG. 10**, showing the correlation between the 3D position error and marker distance from the isocenter. The fitted solid line can be approximated as $y = 0.01x$ in MATLAB with the

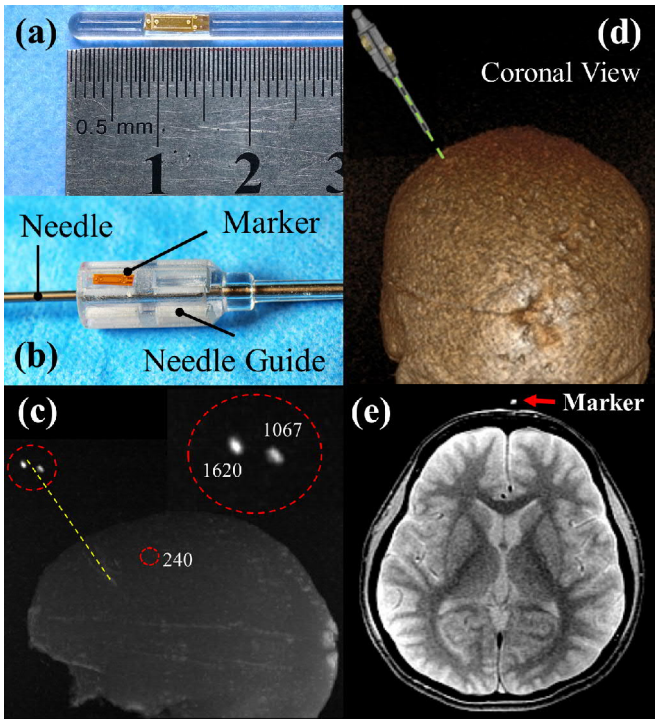

FIG. 13. **(a)** A 3D-printed Ø3-mm catheter embedded with a tracking marker. The small form factor of our marker enables seamless integration with very thin interventional tools. **(b)** Two MR tracking markers embedded in a needle guide, with one visible in the figure. **(c)** MR image of a brain phantom primarily made of agar gel, around which the two bright spots indicate location of the markers. A low-flip-angle pulse sequence was applied. The marker and brain phantom image intensities are indexed with white figures, showing the signal difference is significant. As the markers can have different degree of coupling to the scanner RF coils, the signals amplified are slightly different. **(d)** Configuration of the needle guide virtually augmented on the markers, showing its position and orientation relative to the 3D reconstructed brain phantom. **(e)** GRE image (TE = 6.1 ms, TR = 400 ms, Slice thickness = 5 mm, matrix = 256×192, flip angle = 10°, FOV = 240 mm × 240 mm, pixel spacing = 0.9375 mm) acquired with the tracking marker setup shown in Fig. 3b fixed to a human head with adhesive tape.

curve fitting tool, at a 48 mm distance from the MRI isocenter, the estimated maximum errors in 3D position was 0.48 mm. Increase in the positional error can be explained by the inhomogeneity of the magnetic field created by the MRI scanner. It can be observed that the actual values were scattered around the solid line and was independent of the marker distance from isocenter. The accuracy of wireless marker tracking is comparable to fiducial marker tracking using morphological image processing [48].

Fig. 11 shows the marker's orientation dependency. The marker's signal intensity decreased when its normal axis was tilted from 0° to 90° along the MRI sagittal plane and reduced to minimum when the normal axis was parallel to the B_0 field at 90°. The result shows that the partial coupling between the marker and scanner RF coils can still provide signal enhancement up to 60°.

C. Radiofrequency safety

The maximum recorded temperature rise (measured at the location of the inductor) shown in **FIG. 12** was less than 0.1°C and did not exceed the 0.6°C temperature limit in accordance to ASTM protocol [35]. It is noteworthy that with the small form factor of our marker, it can be easily integrated into applications listed in **TABLE I**. In our current study, two

applications have been developed as shown in **FIG 13**. The first is a Ø3-mm MR-tracked catheter with marker attached onto its surface (**FIG. 13a)**. The second is an 3D-printed needle guide prototyped for a stereotactic procedure [49] (**FIG. 13b)**, which can be visualized and tracked inside the MR image, as depicted in **FIG. 13c-d**.

IV. Conclusion

This paper presents the design, fabrication, and evaluation of a wireless MR-tracking marker, in particular for integration with intra-op MRI-guided interventional tools. Unlike external positional camera tracking systems [2], the proposed marker does not require line-of-sight to the MRI bore, nor any cross-calibration with the MRI scanner. This is because the 3-D positional measurement can be carried out directly in the MR image coordinate system.

Our studies have shown that our novel multilayer design can provide sensitive tracking with a quality factor of 28.5, while achieving a smaller form factor than prior art. It should be noted that a further reduction of form-factor is possible with state of the art FPC manufacturing methods that provide finer trace widths (e.g. 1 mil) and smaller via plating (e.g. 0.2 mm).

The estimated maximum position error was 0.48 mm when the marker was placed 48 mm from the isocenter, and the low standard deviation (0.12 mm) between repeated measurements at the isocenter demonstrates the high repeatability of the position tracking. Note that by using more than 3 markers with known geometrical layout, it can even provide 6 degrees of freedom tracking of a rigid body in 3D, as previously reported for tracking a pair of glasses [29]. The proposed high-sensitivity tracking can be conducted through the use of MR tracking pulse sequences with flip angle of 1°. The current advances of tracking sequence with small temporal footprint [28, 29] can also enable such positional tracking to temporally interleave with imaging sequences. Thereby, navigation of instruments can be facilitated under real-time MRI.

Furthermore, the marker design has minimal hindrance on regular surgical workflow as it does not require additional hardware or external wiring to the MRI scanner. The proposed tracking coil will have a broad range of applications, particularly in MRI-guided robotic interventions such as stereotactic neurosurgery [49], brachytherapy [16], and breast or prostate biopsy. To realize intra-op instrument navigation for such procedures, design of automated and real-time tracking sequence is of importance and is among our pursuits in future work. The tracking marker can also be used to complement the signal of existing MRI navigator methods, which are used to dynamically track anatomical motion. For example, the marker can be placed on the skin of a patient's head for prospective motion correction during brain imaging.

V. References

[1] W. M. Gedroyc, "Interventional magnetic resonance imaging," *BJU Int*, vol. 86 Suppl 1, pp. 174-80, Jul 2000.

[2] M. Moche, R. Trampel, T. Kahn, and H. Busse, "Navigation concepts for MR image-guided interventions," *J Magn Reson Imaging*, vol. 27, no. 2, pp. 276-91, Feb 2008.

[3] M. Borot de Battisti *et al.*, "Fiber Bragg gratings-based sensing for real-time needle tracking during MR-guided brachytherapy," (in eng), *Med Phys*, vol. 43, no. 10, p. 5288, Oct 2016.

[4] L. N. Baldwin, K. Wachowicz, S. D. Thomas, R. Rivest, and B. G. Fallone, "Characterization, prediction, and correction of geometric distortion in 3T MR images," *Medical Physics*, vol. 34, no. 2, pp. 388-399, 2007.

[5] C. J. Bakker, R. M. Hoogeveen, J. Weber, J. J. van Vaals, M. A. Viergever, and W. P. Mali, "Visualization of dedicated catheters using fast scanning techniques with potential for MR-guided vascular interventions," *Magnetic Resonance in Medicine*, vol. 36, no. 6, pp. 816-820, 1996.

[6] D. L. Rubin, A. V. Ratner, and S. W. Young, "Magnetic susceptibility effects and their application in the development of new ferromagnetic catheters for magnetic resonance imaging," (in eng), *Invest Radiol*, vol. 25, no. 12, pp. 1325-32, Dec 1990.

[7] R. A. Omary *et al.*, "Real-Time MR Imaging-guided Passive Catheter Tracking with Use of Gadolinium-filled Catheters," *Journal of Vascular and Interventional Radiology*, vol. 11, no. 8, pp. 1079-1085.

[8] O. Unal, J. Li, W. Cheng, H. Yu, and C. M. Strother, "MR-visible coatings for endovascular device visualization," *Journal of Magnetic Resonance Imaging*, vol. 23, no. 5, pp. 763-769, 2006.

[9] S. Patil, O. Bieri, P. Jhooti, and K. Scheffler, "Automatic slice positioning (ASP) for passive real-time tracking of interventional devices using projection-reconstruction imaging with echo-dephasing (PRIDE)," *Magnetic Resonance in Medicine*, vol. 62, no. 4, pp. 935-942, 2009.

[10] C. L. Dumoulin, S. P. Souza, and R. D. Darrow, "Real-time position monitoring of invasive devices using magnetic resonance," *Magnetic Resonance in Medicine*, vol. 29, no. 3, pp. 411-415, 1993.

[11] F. Galassi, D. Brujic, M. Rea, N. Lambert, N. Desouza, and M. Ristic, "Fast and accurate localization of multiple RF markers for tracking in MRI-guided interventions," (in English), *Magnetic Resonance Materials in Physics, Biology and Medicine*, vol. 28, no. 1, pp. 33-48, 2015/02/01 2015.

[12] N. V. Tsekos, A. Khanicheh, E. Christoforou, and C. Mavroidis, "Magnetic resonance-compatible robotic and mechatronics systems for image-guided interventions and rehabilitation: a review study," (in eng), *Annu Rev Biomed Eng*, vol. 9, pp. 351-87, 2007.

[13] K. H. Lee *et al.*, "MR Safe Robotic Manipulator for MRI-guided Intra-cardiac Catheterization," *IEEE/ASME Transactions on Mechatronics*, vol. PP, no. 99, pp. 1-1, 2018.

[14] K. W. Kwok, Z. Dong, Z. Guo, K. C. D. Fu, K. H. B. Lee, and C. L. Cheung, "Robotic catheter system for mri-guided cardiovascular interventions," US, 2017.

[15] C. L. Dumoulin, S. P. Souza, and R. D. Darrow, "Real-Time Position Monitoring of Invasive Devices Using Magnetic-Resonance," (in English), *Magnetic Resonance in Medicine*, vol. 29, no. 3, pp. 411-415, Mar 1993.

[16] Y. Chen *et al.*, "Design and Fabrication of MR-Tracked Metallic Stylet for Gynecologic Brachytherapy," *IEEE/ASME Transactions on Mechatronics*, vol. 21, no. 2, pp. 956-962, 2016.

[17] M. Bock *et al.*, "MR-guided intravascular procedures: real-time parameter control and automated slice positioning with active tracking coils," (in eng), *J Magn Reson Imaging*, vol. 19, no. 5, pp. 580-9, May 2004.

[18] H. H. Quick *et al.*, "Interventional magnetic resonance angiography with no strings attached: Wireless active catheter

visualization," *Magnetic Resonance in Medicine*, vol. 53, no. 2, pp. 446-455, 2005.

[19] M. E. Ladd and H. H. Quick, "Reduction of resonant RF heating in intravascular catheters using coaxial chokes," (in eng), *Magn Reson Med*, vol. 43, no. 4, pp. 615-9, Apr 2000.

[20] S. Weiss, P. Vernickel, T. Schaeffter, V. Schulz, and B. Gleich, "Transmission line for improved RF safety of interventional devices," (in eng), *Magn Reson Med*, vol. 54, no. 1, pp. 182-9, Jul 2005.

[21] S. Weiss *et al.*, "In vivo safe catheter visualization and slice tracking using an optically detunable resonant marker," *Magn Reson Med*, vol. 52, no. 4, pp. 860-8, Oct 2004.

[22] E. Y. Wong, Q. Zhang, J. L. Duerk, J. S. Lewin, and M. Wendt, "An optical system for wireless detuning of parallel resonant circuits," (in eng), *J Magn Reson Imaging*, vol. 12, no. 4, pp. 632-8, Oct 2000.

[23] M. Detert, M. Kaiser, S. Friesecke, G. Rose, and B. Schmidt, "Evaluation of the hot embossing technology for the fabrication of resonant circuits as instrument visualization method for interventional magnetic resonance imaging," in *2013 Eurpoean Microelectronics Packaging Conference (EMPC)*, 2013, pp. 1-5.

[24] D. Ellersiek *et al.*, "A monolithically fabricated flexible resonant circuit for catheter tracking in magnetic resonance imaging☆," *Sensors and Actuators B: Chemical*, vol. 144, no. 2, pp. 432-436, 2010.

[25] M. Rea, D. McRobbie, H. Elhawary, Z. T. H. Tse, M. LampÉrth, and I. Young, "System for 3-D Real-Time Tracking of MRI-Compatible Devices by Image Processing," *IEEE/ASME Transactions on Mechatronics*, vol. 13, no. 3, pp. 379-382, 2008.

[26] M. Burl, G. A. Coutts, and I. R. Young, "Tuned fiducial markers to identify body locations with minimal perturbation of tissue magnetization," *Magnetic Resonance in Medicine*, vol. 36, no. 3, pp. 491-493, 1996.

[27] M. A. Rube *et al.*, "Preclinical feasibility of a technology framework for MRI-guided iliac angioplasty," *Int J Comput Assist Radiol Surg*, vol. 10, no. 5, pp. 637-50, May 2015.

[28] M. A. Rube, A. B. Holbrook, B. F. Cox, J. G. Houston, and A. Melzer, "Wireless MR tracking of interventional devices using phase-field dithering and projection reconstruction," *Magn Reson Imaging*, vol. 32, no. 6, pp. 693-701, Jul 2014.

[29] M. B. Ooi, M. Aksoy, J. Maclaren, R. D. Watkins, and R. Bammer, "Prospective motion correction using inductively coupled wireless RF coils," *Magn Reson Med*, vol. 70, no. 3, pp. 639-47, Sep 2013.

[30] E. Atalar, "Catheter Coils," in *eMagRes*: John Wiley & Sons, Ltd, 2011.

[31] W. R. Nitz, A. Oppelt, W. Renz, C. Manke, M. Lenhart, and J. Link, "On the heating of linear conductive structures as guide wires and catheters in interventional MRI," (in eng), *J Magn Reson Imaging*, vol. 13, no. 1, pp. 105-14, Jan 2001.

[32] W. R. Nitz, G. Brinker, D. Diehl, and G. Frese, "Specific Absorption Rate as a Poor Indicator of Magnetic Resonance-Related Implant Heating," *Investigative Radiology*, vol. 40, no. 12, pp. 773-776, 2005.

[33] A. Buecker, "Safety of MRI-guided vascular interventions," (in eng), *Minim Invasive Ther Allied Technol*, vol. 15, no. 2, pp. 65-70, 2006.

[34] A. Alipour, S. Gokyar, O. Algin, E. Atalar, and H. V. Demir, "An inductively coupled ultra-thin, flexible, and passive RF resonator for MRI marking and guiding purposes: Clinical feasibility," *Magn Reson Med*, vol. 80, no. 1, pp. 361-370, Jul 2018.

[35] ASTM F2182-09, Standard Test Method for Measurement of Radio Frequency Induced Heating Near Passive Implants During Magnetic Resonance Imaging, ASTM International, West Conshohocken, PA, 2009.

[36] R. P. Feynman, R. B. Leighton, and M. L. Sands, *The Feynman Lectures on Physics* (no. v. 3). Pearson/Addison-Wesley, 1963.

[37] T. Kuehne, R. Fahrig, and K. Butts, "Pair of resonant fiducial markers for localization of endovascular catheters at all catheter orientations," *J Magn Reson Imaging*, vol. 17, no. 5, pp. 620-4, May 2003.

[38] M. Rea, D. McRobbie, H. Elhawary, Z. T. Tse, M. Lamperth, and I. Young, "Sub-pixel localisation of passive micro-coil fiducial markers in interventional MRI," (in eng), *Magma*, vol. 22, no. 2, pp. 71-6, Apr 2009.

[39] W. Wang *et al.*, "Real-time active MR-tracking of metallic stylets in MR-guided radiation therapy," *Magn Reson Med*, vol. 73, no. 5, pp. 1803-11, May 2015.

[40] W. G. Hurley and M. C. Duffy, "Calculation of self- and mutual impedances in planar sandwich inductors," (in English), *IEEE Transactions on Magnetics*, vol. 33, no. 3, pp. 2282-2290, May 1997.

[41] W. G. Hurley, M. C. Duffy, S. O'Reilly, and S. C. Mathuna, "Impedance formulas for planar magnetic structures with spiral windings," (in English), *IEEE Transactions on Industrial Electronics*, vol. 46, no. 2, pp. 271-278, Apr 1999.

[42] S. Babic and C. Akyel, "Improvement in calculation of the self- and mutual inductance of thin-wall solenoids and disk coils," (in English), *IEEE Transactions on Magnetics*, vol. 36, no. 4, pp. 1970-1975, Jul 2000.

[43] F. W. Grover, *Inductance Calculations: Working Formulas and Tables*. Dover Publications, 2004.

[44] S. Babic, F. Sirois, C. Akyel, and C. Girardi, "Mutual Inductance Calculation Between Circular Filaments Arbitrarily Positioned in Space: Alternative to Grover's Formula," (in English), *IEEE Transactions on Magnetics*, vol. 46, no. 9, pp. 3591-3600, Sep 2010.

[45] S. I. Babic and C. Akyel, "New analytic-numerical solutions for the mutual inductance of two coaxial circular coils with rectangular cross section in air," (in English), *IEEE Transactions on Magnetics*, vol. 42, no. 6, pp. 1661-1669, Jun 2006.

[46] W. G. Hurley, M. C. Duffy, J. Zhang, I. Lope, B. Kunz, and W. H. Wolfle, "A Unified Approach to the Calculation of Self- and Mutual-Inductance for Coaxial Coils in Air," (in English), *IEEE Transactions on Power Electronics*, vol. 30, no. 11, pp. 6155-6162, Nov 2015.

[47] J. Uei-Ming and M. Ghovanloo, "Modeling and optimization of printed spiral coils in air, saline, and muscle tissue environments," *IEEE Trans Biomed Circuits Syst*, vol. 3, no. 5, pp. 339-47, Oct 2009.

[48] H. Busse, R. Trampel, W. Grunder, M. Moche, and T. Kahn, "Method for automatic localization of MR-visible markers using morphological image processing and conventional pulse sequences: feasibility for image-guided procedures," *J Magn Reson Imaging*, vol. 26, no. 4, pp. 1087-96, Oct 2007.

[49] Z. Guo *et al.*, "Compact Design of a Hydraulic Driving Robot for Intra-operative MRI-guided Bilateral Stereotactic Neurosurgery," *IEEE Robotics and Automation Letters*, To be appeared, 2018.

Chim-Lee Cheung received the B.Eng. degree in electrical engineering from The University of Hong Kong, Hong Kong, in 2015, where he is currently working toward the Ph.D. degree in medical robotics. His research interests include the design and fabrication of intraoperative magnetic resonance imaging tracking devices for robot-assisted system.

Justin Di-Lang Ho received the M.Phil. from Department of Mechanical Engineering at The University of Hong Kong (HKU). He received a bachelor's degree with an extended major in Mechatronic Engineering at the University of Queensland (UQ), Australia in 2016. His primary research interests are in soft robotics, MRI-guided robotics, fibre-optic sensing, and augmented reality for surgery.

Vince Vardhanabhuti completed his medical degree at Guy's, King's and St Thomas' School of Medicine in London, UK in 2005. He had subsequent training in London, Oxford, Plymouth, Exeter, and completed his Radiology training at Imperial College Healthcare NHS Trust in London, UK. He has been working at the Department of Diagnostic Radiology at the University of Hong Kong since 2014 as a Radiologist and Clinical Assistant Professor. He has active research interests in MRI and engages with various research projects relating to medical imaging, with the goal of early clinical translation to benefits patients.

Hing-Chiu Chang received the B.S. and M.S. degrees in electrical engineering from the National Taiwan University, Taiwan, in 2004 and 2006, respectively, and the Ph.D. degree from the Graduate Institute of Biomedical Electronics and Bioinformatics, National Taiwan University, Taiwan, in 2012. He spent 6 years working for medical imaging industry. He is currently a Research Assistant Professor of the Department of Diagnostic Radiology at The University of Hong Kong. His research interests include image reconstruction and artifact reduction for fast magnetic resonance imaging.

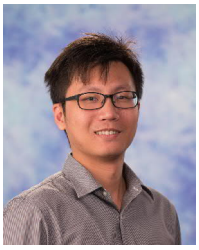

Ka-Wai Kwok received the B.Eng. and MPhil. from Department of Automation and Computer-Aided Engineering, The Chinese University of Hong, and then the Ph.D. degree from Hamlyn Centre for Robotic Surgery, Department of Computing, Imperial College London in 2012. He is currently an Assistant Professor in Department of Mechanical Engineering, The University of Hong Kong. His research interests include designs of surgical robotic devices, and their control interface for endoscopy, laparoscopy, stereotactic, and intracardiac catheter interventions. Dr. Kwok has been recognized by several awards from IEEE international conferences, for example, Best Conference Paper Award of 2018 International Conference on Robotics and Automation (ICRA), and First Place Prize Paper Award in the 2017 IEEE Transactions on Power Electronics (TPEL), as well as RCAR'17, ICRA'17, ICRA'14, IROS'13, and FCCM'11. He also received Early Career Awards 2015/2016 offered by the Research Grants Council of Hong Kong.